Comparing Orientation-Dependent Transverse Relaxation at 3 T and 7 T: Deciphering Anisotropic Relaxation Mechanisms in White Matter

Yuxi Pang, Rajikha Raja, and Wilburn E. Reddick

Department of Radiology,

St. Jude Children's Research Hospital, Memphis, TN, USA

Corresponding Author:

Yuxi Pang, PhD

Department of Radiology

St. Jude Children's Research Hospital

262 Danny Thomas Place, MS 220

Memphis, TN, 38105-3678 USA

Email: yuxi.pang@stjude.org

ORCID ID: https://orcid.org/0000-0001-5039-0236

Running Title: Comparing Orientation-Dependent Transverse Relaxation at 3 T and 7 T

Word Count: 4863

St. Jude - Confidential

1 | INTRODUCTION

The distinct contrasts observed in magnetic resonance (MR) imaging of biological tissues are strongly influenced by the composition of biomolecular constituents and their hierarchical organization [1, 2]. Multiple relaxation mechanisms—including (residual) dipolar interactions, chemical exchange, and (anisotropic) susceptibility effects—contribute to these image contrasts. For example, both susceptibility-based pathways and the magic angle effect (MAE) have recently been considered [3] for characterizing orientation-dependent transverse relaxation in brain white matter (WM). However, MAE has not been adequately addressed, largely due to an oversight of the detailed organization of bound water adjacent to or within biomacromolecules. Historically, the concept of "structured" water in tissues has been met with skepticism [4]; nevertheless, its recent application via MAE to orientation-dependent transverse relaxometry in neural tissues [5, 6] has highlighted the role of microstructural water organization, challenging previously prevalent susceptibility-based models [3, 7, 8].

Approximately two decades ago, the increasing availability of whole-body MR scanners operating at ultra-high magnetic B_0 fields led to the discovery of unprecedented varying T_2^* contrast in gradient-echo (GRE) images of human brain WM in vivo at 7 T [9, 10]. This characteristic T_2^* contrast (or its reciprocal, R_2^* contrast) was subsequently found to depend on the orientation of axon fiber tracts in an animal study [11], where the anesthetized brain was positioned at different angles relative to the B_0 field. Shortly thereafter, a clearer picture emerged from a study conducted on healthy human brains at 3 T [12], where the R_2^* values in fiber tracts were found to be higher along either the left-right or anterior-posterior directions compared to the inferior-superior direction, which aligns with the B_0 field. Moreover, the observed R_2^* values appeared to

St. Jude - Confidential

be proportionally correlated with diffusion fractional anisotropy (FA) derived from diffusion tensor imaging (DTI).

The complete profiles of R_2^* orientation dependence in human brain WM in vivo at 3 T were eventually established by leveraging orientation information from DTI, specifically using the principal diffusivity (λ_1) direction within each imaging voxel [13, 14]. More importantly, an orientation-dependent function of $\sin^2\theta$ (or equivalently $\sin 2\theta$ [15]) was proposed, where θ is the angle between the λ_1 direction and the B_0 field. In a subsequent study involving two coronal formalin-fixed brain slabs at 7 T [16], an enhanced orientation-dependent function was developed, incorporating an additional $\sin 4\theta$ term. This refined function was derived from R_2^* measurements of brain specimens rotated at 18 different angles around the brain slab's norm direction, spanning from 0° to 170° relative to the B_0 field. In this ex vivo study, the investigators also introduced a phase shift (φ_0) into the proposed R_2^* orientation-dependent function. However, the biophysical basis of φ_0 was not adequately elucidated. As a result, this phase shift was often overlooked in subsequent applications of the function to previously reported studies, where orientation information was derived from λ_1 in DTI [17-19].

To better understand the origins of the observed orientation-dependent transverse relaxation in WM, a follow-up investigation was conducted at 7 T using rotating brain specimens, following a workflow similar to that described above [3]. In this comparative study, unlike the pronounced R_2^* orientational anisotropy, the measured R_2 values exhibited minimal, if any, discernible orientation dependence. This observation led investigators to conclude that magnetic susceptibility effects were the dominant mechanism underlying anisotropic relaxation. However, the temperature-dependent anisotropies of R_2^* observed in the brain samples could not be adequately explained by the proposed relaxation mechanism, because the diamagnetic

St. Jude - Confidential

susceptibility of myelin is essentially independent of temperature and the static dephasing theory invoked therein also neglects spin motion. These conflicting findings clearly illustrate that the true origin of orientation-dependent R_2^* in WM remains elusive.

Meanwhile, researchers developed a hollow cylinder fiber model (HCFM) for WM based on magnetic susceptibility theory [7, 20]. In this model, the annular region of the cylinder is filled with molecular constituents exhibiting anisotropic magnetic susceptibilities, allowing prediction of R_2^* orientation dependence using an analytical function that includes a $\sin^4\theta$ or $\sin 4\theta$ term [7]. However, this analytical function alone was insufficient to accurately characterize the shape of orientation-dependent R_2^* profiles measured from rotating pig brain samples, unless an additional heuristic $\sin^2\theta$ term was included. Interestingly, a similar orientation-dependent R_2 function, which incorporates the term $\sin^4\theta$, with and without the term $\sin^2\theta$, was also proposed for human brain WM in vivo at 3 T [8]. The underlying biophysical principle of the proposed model for R_2 orientational anisotropy was the same susceptibility theory for R_2^* anisotropy but applied at a mesoscopic scale. Specifically, diffusion-mediated decoherence, arising from local susceptibility variations across axon fiber bundles, enhances the transverse relaxation measured at the macroscopic voxel level.

Another potential anisotropic relaxation mechanism is the well-known MAE [21], originated from rotationally restricted water molecules in highly ordered biological tissues [22], but this effect has not been adequately considered in existing orientation-dependent R_2^* or R_2 relaxation models [16, 23]. This oversight is partially due to the markedly different profiles of measured R_2^* or R_2 orientation dependence in WM, where enhanced relaxation rates are observed when axon fibers are oriented perpendicular to the B_0 field, compared to parallel [12]. In contrast, conventional MAE profiles, such as those observed in tendons and deep-zone cartilage, exhibit the

St. Jude - Confidential

opposite pattern of transverse relaxation rate enhancement between these two orientations [21]. Recently, this seemingly contradictory R_2^* or R_2 anisotropy in WM has been reconciled by employing a generalized MAE function that incorporates a phase shift [5, 6]. Remarkably, the proposed MAE-based function can be reformulated in terms of previously developed orientation-dependent R_2^* and R_2 models, thereby suggesting a potentially ambiguous mechanism underlying anisotropic transverse relaxation in WM, as reported in prior literature [3, 15].

An orientation-dependent transverse relaxation rate provides essential specificity in neuro-microstructural imaging, as it directly reflects the extent of (de)myelination in WM [3, 5, 20, 24]. To accurately capture the underlying biophysical processes, it is essential to disentangle the previously proposed relaxation mechanisms—namely, the susceptibility effects and the MAE—in relation to R_2^* and R_2 orientational anisotropies. These two competing anisotropic relaxation pathways exhibit distinct B_0 field dependences: susceptibility effects scale with B_0^2, whereas the MAE is independent of B_0. Consequently, these mechanisms can, in principle, be distinguished by comparing orientation-dependent R_2 across different B_0 field strengths. This separation is critical for advancing our understanding of the unique anisotropic relaxation signatures associated with the highly organized microstructures in WM. Given the current ambiguity surrounding the mechanism of orientation-dependent transverse relaxation, this work aims to clarify the long-standing question regarding the origins of anisotropic transverse relaxation in human brain WM by examining orientation-dependent R_2 values derived from both spin-echo and gradient-echo measurements at 3 T and 7 T, as previously published in the literature. Compared to our prior investigations [5, 6], this study represents a significant advance by identifying the dominant anisotropic relaxation pathway at clinically widely available B_0 field strengths.

St. Jude - Confidential

2 | THEORY

This section provides a brief overview of previously developed biophysical models describing the orientation dependence of R_2^* and R_2 in brain WM. The literature indicates that the orientation dependence of R_2^*—which equals $R_2 + R_2'$—originates primarily from R_2 rather than R_2' [7, 25]. It is generally accepted that R_2' arises mainly from non-local effects caused by large length-scale B_0 inhomogeneities and macroscopic variations in magnetic susceptibility [7]. Because this non-local contribution is time-independent, it can be removed during post-processing when deriving the orientation dependence of R_2^*.

Minor anisotropic R_2' contributions may arise from WM boundaries; however, the data-binning workflow used in this study would likely reduce their potential impact. Nevertheless, this issue should be carefully considered in ex vivo studies of brain WM samples. Accordingly, in the present study, R_2^* and R_2 are treated interchangeably with respect to orientation dependence, even though they are derived from GRE and spin-echo (SE) datasets, respectively. This approach is consistent with previous reports [6, 25].

2.1 | Susceptibility-based models for R_2^* and R_2 orientation dependences

According to the previously proposed HCFM model [7, 20], an orientation-dependent function for R_2^* is given in Equation 1, which includes an analytically derived term $\sin^4\theta$ and a heuristic term $\sin^2\theta$. The latter term is essential for accounting for myelin water contributions to both simulated and observed R_2^* values in WM [7]. A seemingly different, yet mathematically equivalent [15], orientation-dependent function for R_2^* has also been developed in the literature [3], as shown in Equation 2:

$$R_2^* = A_0 + A_1 \sin^2\theta + A_2 \sin^4\theta \qquad [1]$$

$$R_2^* = B_0 + B_1 \cos 2\theta + B_2 \cos 4\theta \qquad [2]$$

St. Jude - Confidential

Although mathematically equivalent, these two functions arise from fundamentally different biophysical assumptions. The $\sin^2\theta$ and $\sin^4\theta$ terms in Equation 1 originate from myelin water in the static dephasing regime and from intra- and extra-axonal water in the diffusion or motional narrowing regime, respectively [7]. In contrast, Equation 2 was derived under the assumption that the measured signals are entirely in the static dephasing regime [26], where translational diffusion is negligible. The $\cos 2\theta$ and $\cos 4\theta$ terms are attributed to the highly ordered myelin microstructure and its associated susceptibility anisotropy [3].

Interestingly, Equation 1 has also been proposed to characterize the orientation dependence of R_2 [8], where the $\sin^4\theta$ term arises from diffusion-mediated decoherence due to mesoscopic magnetic susceptibility differences, and the $\sin^2\theta$ term results from interactions between susceptibility differences and applied field gradients. While the latter contribution is expected to be negligible in standard SE datasets, it appears necessary to include the $\sin^2\theta$ term to better fit the orientation dependence profile of R_2 in WM [15, 19].

2.2 | A generalized orientation-dependent model derived from MAE

Given the conflicting biophysical foundations of previously developed models, a generalized orientation-dependent function has been proposed for WM that relies solely on the well-established MAE [5, 6]. As schematically illustrated in Figure 1A (adapted from the literature [27]), a typical myelinated axon is wrapped in multiple layers of bilayer membranes. Rotationally restricted water can reside both within an axonal space [17, 28], denoted by a filled violet circle, and in the compartments containing myelin water [29], indicated by the label H2O (Figure 1B). In the latter case, the *intramolecular* proton-proton (H-H) residual dipolar interaction (RDI) vectors from rotationally restricted water are assumed to lie within the plane perpendicular to the axon axis (Figures 1A-1C) [5]. In contrast, the RDI vectors within the axonal space are assumed to align

St. Jude - Confidential

along the axon's longitudinal axis [17]. These two extreme cases correspond to the RDI vector distributions in ideal collagen fiber organizations in the superficial (tangential) and deep (radial) zones [30, 31].

A generalized function was derived by evaluating the effective RDI vectors within an axially symmetric system, modeled as a cone (Figure 1E) with an opening angle α. This angle represents the relative contributions from water inside (α = 0°) and outside (α = 90°) the axon (Figure 1D) [5]. In this model, the effective RDI vectors, characterized by the orientation-dependent term $(3\cos^2\theta - 1)^2$, are distributed along the cone wall. If the cone's axis forms an angle ε with respect to the B_0 field, the orientation dependence of R_2 from this ensemble of RDI vectors can be concisely expressed as [5, 6]:

$$f(\alpha, \varepsilon) = \frac{1}{4}(3\cos^2\alpha - 1)^2(3\cos^2\varepsilon - 1)^2 + \frac{9}{8}(\sin^4\alpha \sin^4\varepsilon + \sin^2 2\alpha \sin^2 2\varepsilon) \qquad (3)$$

It has previously been shown that Equations 1-3 are mathematically equivalent, differing only in their scaling factors [6, 15]. When α = 0°, this generalized function reduces to the conventional MAE expression: $f(0°, \varepsilon) = (3\cos^2\varepsilon - 1)^2$. Conversely, when α = 90°, this function becomes: $f(90°, \varepsilon) = (1/4)(3\cos^2\varepsilon - 1)^2 + (9/8)(\sin^4\varepsilon)$. As shown in Figure 1F, the orientation-dependent profile of $f(0°, \varepsilon)$ (black curve) differs markedly from that of $f(90°, \varepsilon)$ (blue curve). Confusion may arise if the observed orientation-dependent measures in WM are interpreted using the conventional MAE expression.

The transverse relaxation rate R_2 measured in WM can generally be decomposed into two components: an orientation-independent term R_2^i, and an orientation-dependent term $R_2^a \cdot f(\alpha, \varepsilon)$, expressed as:

$$R_2 = R_2^i + R_2^a \cdot f(\alpha, \varepsilon) \qquad (4)$$

St. Jude - Confidential

In this formulation, R_2^a represents the magnitude of the orientation dependence, which reaches its maximum value of $4R_2^a$ when both α and ε are zero [6].

When considering an effective transverse relaxation rate R_2^*, defined as $R_2 + R_2'$, the contribution from R_2' is incorporated into the orientation-independent term R_2^i. It is important to note that R_2^i is typically assumed to be constant when analyzing orientation-dependent phenomena in biological tissues.

2.3 | Orientation dependence of R_2 derived from a single T_2-weighted image

As shown in the literature [5, 6], R_2^a can be extracted from T2W images when voxel-wise fiber orientations (ε) are available. The signal of a typical voxel ($S_{b=0}$) in a T2W image can be expressed as

$$S_{b=0} = M_0 exp\left[-\left(R_2^i + R_2^a \cdot f(\alpha, \varepsilon)\right) \cdot TE\right] \qquad (5)$$

Here, M_0 is the maximum signal amplitude as TE approaches zero. In logarithmic form, Equation 5 can be rewritten as

$$\ln(S_{b=0})/TE = C_0 - R_2^a \cdot f(\alpha, \Phi - \varepsilon_0) \qquad (6)$$

where C_0 is an unknown constant defined as $\ln(M_0)/TE - R_2^i$, ε_0 is a phase shift [6], and Φ denotes the principal diffusivity direction relative to the B_0 field (see Section 3.1).

As previously reported, M_0 varies minimally across WM throughout the brain [32] and is therefore treated as constant. It is worth noting that the definition of M_0 may be susceptible to some T_1 effects, which have also been reported to be orientation-dependent [33]. However, these potential effects are negligible, as the degree of R_1 (=$1/T_1$) anisotropy is at least two orders of magnitude smaller than that of R_2 anisotropy.

2.4 | B_0-dependence of anisotropic transverse relaxation rates

St. Jude - Confidential

As shown above, Equations 1-3 are mathematically equivalent when scaling factors are not considered, yet they are derived from distinct biophysical foundations. Therefore, it is not feasible to disentangle two different relaxation mechanisms in WM merely by rearranging orientation-dependent terms in previously proposed model functions [3, 15]. If magnetic susceptibility were the sole mechanism driving orientation-dependent relaxation, then R_2^a would be expected to scale proportionally with B_0^2 [7, 8]. Conversely, if MAE were responsible for anisotropic transverse relaxation, then R_2^a would be entirely independent of B_0 [22, 34].

Accordingly, these two relaxation mechanisms can be disentangled by comparing R_2^a values measured at two different magnetic field strengths, as demonstrated in the literature [35]. For example, the ratio between R_2^a measured at 7 T and 3 T, denoted by η, is theoretically predicted to be $\eta = (7/3)^2 = 5.44$, assuming the increase in R_2^a is solely due to susceptibility effects. When considering the actual B_0 field strengths used in data acquisitions [36], i.e., 2.895 T and 6.980 T, η increases slightly to 5.81. This more realistic value is used in the following data analysis, although the field strengths will continue to be referred to as 3 T and 7 T for convenience.

In a different scenario, susceptibility may partially contribute to the observed R_2^a in WM. In this case, the percentage contribution of susceptibility to the measured R_2^a at 3 T can be quantified as described in the literature [35]: $100 \cdot \Delta R_2^a / (R_2^a(3T) \cdot (\eta - 1))$, where $\Delta R_2^a = R_2^a(7T) - R_2^a(3T)$. Similarly, the partial contribution to the measured R_2^a at 7 T can be evaluated as: $100 \cdot (\eta \cdot \Delta R_2^a) / (R_2^a(7T) \cdot (\eta - 1))$. Nonetheless, any conclusion regarding the relative importance of specific anisotropic transverse relaxation mechanisms should remain consistent, regardless of whether R_2^a is measured using GRE or SE signals.

3 | METHODS

St. Jude - Confidential

3.1 | Publicly available DTI datasets at 3 T and 7 T from HCP

After signing the data usage agreement, we randomly selected 25 participants from a cohort of 184 young adults in the Human Connectome Project (HCP) [https://www.humanconnectome.org/study/hcp-young-adult]. Each subject had DTI datasets acquired at both 3 T (TE = 89 ms) and 7 T (TE = 71 ms). As shown in Tables S1 and S2, each subject is identified by a subject number (1st column) used in the present study, along with their HCP-ID (2nd column), which specifies the original HCP identification number, gender, and age. For example, the 15th subject's HCP-ID is 385046, the gender is male (M), and the age is 28 years.

These publicly available DTI datasets had already been preprocessed to correct image artifacts caused by signal drift, susceptibility effects, eddy currents, gradient nonlinearity-induced distortions, and involuntary head motion. Data subsets with b-values of 0 and 1000 s/mm^2, as well as b-values of 0 and 2000 s/mm^2, were separately fitted using FSL's DTIFIT software [37]. In other words, each participant contributed two datasets at a specific field strength. The fitted parameters included three eigenvalues (λ_1, λ_2, λ_3), three eigenvectors ($\hat{e}_1$, $\hat{e}_2$, $\hat{e}_3$), fractional anisotropy (FA), mode of anisotropy (MO) [38], and T_2-weighted (T2W) images. The direction Φ of the principal diffusivity λ_1, relative to the B_0 field, was represented by the primary eigenvector $\hat{e}_1$ using the relationship [13, 19]: $\cos\Phi = \hat{e}_1 \cdot \vec{B}_0 / \|\hat{e}_1 \cdot \vec{B}_0\|$.

WM voxels were segmented from high-resolution anatomical T_1-weighted volumetric images in the HCP datasets. These voxels were further refined using thresholds of 0.5 < FA < 0.9 and 0.5 < MO < 1.0, ensuring that each WM voxel was well-characterized by a prolate diffusion tensor [6]. Note that M_0 and MO refer to distinct entities. Figure 2 shows the final WM masks superimposed on T2W images from DTI acquired at 3 T and 7 T. After pooling and binning data from the selected WM voxels across the brain, orientation-dependent profiles of $R_2^a \cdot f(\alpha, \Phi -$

ε_0), defined as $C_0 - \ln(S_{b=0})/TE$, were established as demonstrated in prior studies [5, 6]. The four model parameters (C_0, R_2^a, α, and ε_0) were extracted using a nonlinear least-squares curve fitting method [39]. In total, fifty orientation-dependent R_2 profiles were generated, with each participant contributing two datasets corresponding to distinct non-zero *b*-values at a specific field strength; this sample size allows reliable conclusions to be drawn.

3.2 | Previously published orientation-dependent R_2^* profiles at 3 T and 7 T

A free online tool (www.graphreader.com) was used to extract previously published orientation-dependent R_2^* profiles of WM at 3 T and 7 T. These profiles were measured either across whole-brain WM or within specific fiber tracts in healthy subjects. The reported R_2^* datasets were acquired in accordance with ethical guidelines, as stated in the original publications.

The first R_2^* profile of whole-brain WM at 3 T [40], free from the confounding flip angle effect (FAE), was derived by linear regression from profiles measured at the flip angles of 6°, 17°, 35° and 60°, as described in the literature [41]. This orientation-dependent R_2^* profile at 3 T, independent of FAE, was averaged across six subjects (age 22-29; median age 25). The second R_2^* profile of whole-brain WM at 7 T, also free from FAE, was extracted directly from Figure 7 (Session2, green) of the original paper [41]. This profile was measured in three healthy subjects (mean age 38.7 ± 4.2 years).

The third and fourth R_2^* profiles were derived from the corpus callosum (CC) at 3 T and 7 T, respectively, while the fifth and sixth profiles were obtained from the cingulum (CG) at 3 T and 7 T [42]. These R_2^* profiles were reported in a conference abstract that did not include specific demographic information. However, a related publication based on partial datasets indicated that five healthy participants were involved, with an average age of 34 ± 6 years [43].

St. Jude - Confidential

It is worth noting that the orientation information underlying the 7 T R_2^* profiles was derived from 3 T DTI data [41, 42]. Furthermore, the orientation used to describe all R_2^* profiles, except for the second, was defined as the angle between the B_0 field and the direction of the first peak of the orientation distribution function (ODF), rather than the direction (Φ) of the principal diffusivity, which is more commonly used. The ODF was previously computed using the constrained spherical deconvolution method applied to multi-shell diffusion datasets [44]. For consistency, these ODF-based angles are still denoted as Φ in this work.

3.3 | Data analysis and error estimations

Orientation-dependent $R_2^a \cdot f(\alpha, \Phi - \varepsilon_0)$ profiles based on single SE signals were generated using custom Python scripts. Each profile consisted of 18 data points, covering orientations (Φ) from 2.5° to 87.5°. A publicly available nonlinear least-squares fitting routine (http://purl.com/net/mpfit) [39], written in Interactive Data Language (IDL 9.1, Harris Geospatial Solutions, Inc., Broomfield, CO, USA), was used to characterize these orientation-dependent profiles based on Equation 6. For profiles derived from GRE signals, the fitting was performed using Equation 4, where the theoretical fiber orientation ε was replaced with $\Phi - \varepsilon_0$.

The fitted model parameters were constrained to the following ranges:

1. SE-based profiles: C_0 = [0, 200] s^{-1} and R_2^a = [0, 10] s^{-1}
2. GRE-based profiles: R_2^i = [0, 100] s^{-1} and R_2^a = [0, 100] s^{-1}
3. All profiles: α = [0°, 90°] and ε_0= [0°, 45°]

Note that R_2^i could not be determined from T2W images acquired with only one TE, as is typically the case in standard DTI datasets. Because the nonlinear least-squares fittings were unweighted, the reported uncertainties, formal 1σ errors in each fitted parameter derived from the

St. Jude - Confidential

covariance matrix, were rescaled such that the reduced χ^2 was approximately unity. More information can be found in the commentary section of the fitting routine (i.e., mpfit.pro).

Unless otherwise stated, error propagation was performed according to the standard procedures as described in [45]. Standard deviations of the presented data are indicated by error bars or by the half-widths of shaded ribbons. Image data were visualized using the MRtrix3 viewer (MRView; Figure 2) [46].

4 | RESULTS

4.1 | R_2^a derived from SE signals at 3 T and 7 T

Figure 3 compares representative orientation (Φ) dependence profiles of $R_2^a \cdot f(\alpha, \Phi - \varepsilon_0)$ between 3 T (blue) and 7 T (red) from the 15th subject (HCP_ID: 385046_M28). These profiles were derived from non-zero *b*-value of 1000 s/mm^2 (Figure 3A) and 2000 s/mm^2 (Figure 3B). For the 1000 s/mm^2 data, the fitted R_2^a increased from 4.16 ± 0.39 s^{-1} at 3 T to 6.27 ± 0.58 s^{-1} at 7 T, while other fit parameters, such as α and ε_0, remained comparable. Comparing Figure 3B with Figure 3A, the fitted R_2^a appears relatively larger at the higher *b*-value. This increase is attributable to the fixed selection thresholds for FA and MO used in this study, as well as the inverse relationship between *b*-value and FA, as discussed in our prior work [6]. The ratio η of R_2^a values between 7 T and 3 T was 1.51 ± 0.20. For the 2000 s/mm^2 data, this ratio (η = 1.60 ± 0.25) was nearly identical, within measurement uncertainties. Notably, these measured η values are significantly lower than the theoretical ratio (η = 5.81) expected if susceptibility effects alone accounted for the observed orientation-dependent transverse relaxation in WM.

Across all 25 subjects included in this study, the fitted R_2^a values at 3 T are plotted against those measured at 7 T in Figure 4, for datasets with *b*-values of 1000 s/mm^2 (Figure 4A) and 2000

St. Jude - Confidential

s/mm^2 (Figure 4C). In these plots, colored dashed lines represent two theoretically predicted η values corresponding to exclusive anisotropic relaxation mechanisms: susceptibility effects (η = 5.81, red) and MAE (η = 1.0, blue). Subject-specific η values are shown in Figure 4B and Figure 4D, with mean values of 1.39 ± 0.50 and 1.47 ± 0.40, respectively, indicated by dashed horizontal lines. Detailed fitted parameters are provided in Table S1 (b-value=1000 s/mm^2) and Table S2 (b-value=2000 s/mm^2).

From 3 T to 7 T, as shown in Table S1, the fitted R_2^a values increased on average from 4.0 ± 1.1 s^{-1} to 5.6 ± 1.6 s^{-1}, corresponding to ΔR_2^a = 1.6 ± 1.9 s^{-1}. The percentage contribution of susceptibility effects to the measured R_2^a at 3 T was 8.3 ± 10.2%, compared with 34.5 ± 42.2% at 7 T. Comparable results were obtained from the fits in Table S2; specifically, the susceptibility-based contributions at 3 T and 7 T were 6.6 ± 10.3% and 29.1 ± 45.6%, respectively,

These results suggest that MAE predominantly contributes to the measured R_2^a at 3 T, consistent with recent findings in the literature [25, 47]. As shown in Table S1, the average fitted α increased from 66.5 ± 2.3° to 69.6 ± 1.8°, while ε_0 decreased from 26.2 ± 3.8° to 11.5 ± 11.0°. These fitted model parameters and their relative changes from 3 T to 7 T are consistent with those reported in Table S2.

4.2 | R_2^a derived from GRE signals at 3 T and 7 T

When comparing the fitted parameters from the orientation-dependent R_2^* profiles of whole-brain WM at 3 T (Figure 5A) and 7 T (Figure 5B), we found that the measured R_2^a values at the two field strengths are comparable within the limits of precision: 6.88 ± 0.32 s^{-1} at 3 T versus 7.05 ± 1.26 s^{-1} at 7 T. Furthermore, no significant differences were observed between 3 T (blue) and 7 T (red) in a separate study from the literature [42], where R_2^a values were derived from specific fiber tracts. For example, in the corpus callosum (CC, Figure 5C), the values were 10.98

St. Jude - Confidential

± 0.74 s^{-1} at 3 T and 9.42 ± 2.91 s^{-1} at 7 T; in the cingulum (CG, Figure 5D), they were 11.03 ± 1.96 s^{-1} at 3 T and 10.22 ± 2.05 s^{-1} at 7 T. These findings suggest that susceptibility effects are not the dominant mechanism underlying anisotropic transverse relaxation, contrary to previous assumptions [3, 7, 8], and consistent with the conclusions discussed above.

5 | DISCUSSION

The aim of this study is to elucidate the long-standing challenges surrounding the origins of orientation-dependent transverse relaxation in human brain WM. By comparing anisotropic transverse relaxation rates observed at 3 T and 7 T using both SE and GRE signals, we disentangled the respective contributions of MAE and susceptibility effects by leveraging their distinct dependences on the main magnetic field strength.

5.1 | Distinct R_2^a values obtained from SE and GRE measurements

Previously reported R_2^a values in human brain WM have exhibited considerable variability across studies. This variability arises not only from differences in data acquisition protocols, such as pulse sequence design, echo spacing, and number of echoes, but also from variations in post-processing strategies, including signal fitting models and region-of-interest selection. For instance [24], Gil et al. demonstrated that R_2^a values derived from multi-echo SE (MESE) signals at 3 T were significantly lower than those obtained from multi-echo GRE (MEGE) signals. Specifically, MESE-based R_2^a values ranged from 0 to 1.5 s^{-1}, while MEGE-based values ranged from 3.1 to 4.5 s^{-1}, underscoring the influence of sequence type on the estimation of anisotropic transverse relaxation.

In the present study, we observed a similar trend. The average R_2^a value derived from single SE signals embedded in DTI datasets was approximately 4.0 s^{-1} (Table S1), which is notably lower

St. Jude - Confidential

than the GRE-derived values of around 7.0 s^{-1} (Figures 5A-5B) for whole-brain WM at both 3 T and 7 T. Moreover, GRE-based values were even higher when the analysis was focused on specific fiber bundles, such as the corpus callosum (Figure 5C) and the cingulum (Figure 5D), indicating that these specific fiber tracts exhibit relatively higher microstructural anisotropies and orientation-dependent relaxation effects.

To mitigate methodological inconsistencies and isolate the influence of magnetic field strength, we restricted our comparison of R_2^a values to datasets acquired using similar pulse sequences and post-processing workflows at both 3 T and 7 T. This approach minimized confounding factors and ensured that the observed differences in R_2^a values primarily reflect true effects associated with field strengths, rather than artifacts introduced by acquisition or analysis variability.

While B_1 field inhomogeneity becomes inevitable across the whole brain at higher field strengths, our analysis focuses exclusively on a subset of WM voxels exhibiting highly organized ($0.5 < FA < 0.9$ and $0.5 < MO < 1.0$) microstructure. These selected voxels, derived from various brain regions, were binned and averaged according to their orientations to generate orientation-dependent R_2 profiles. This customized processing workflow is expected to reduce the potential impact of B_1 inhomogeneity on our results.

5.2 | B_0-dependent R_2^a from SE signals

Based on single SE signals acquired from whole-brain WM in 25 subjects, we observed an average increase in R_2^a from 3 T to 7 T of $\Delta R_2^a = 1.6 \pm 1.9$ s^{-1}, indicating a modest, though not dominant, as previously assumed, contribution of susceptibility effects to the measured R_2^a at 3 T. This contribution was estimated at 8.3 ± 10.2%, suggesting that while susceptibility effects are

St. Jude - Confidential

present, they account for only a minor portion of the anisotropic transverse relaxation at this field strength.

This finding is consistent with prior results from B_0-dependent $T_{1\rho}$ dispersion studies in rat brain WM [5, 48], in which susceptibility effects accounted for approximately 12% of the transverse relaxation dispersion at 3 T [5], with the remaining contrast attributed to MAE. Supporting this interpretation, Bauser et al. recently reported negligible changes in orientation-dependent R_2 of single-fiber WM voxels between 1.5 T and 3 T using MESE measurements [47], further reinforcing the notion that MAE is the dominant mechanism driving anisotropic transverse relaxation at lower field strengths.

It is worth emphasizing, however, that Bauser et al. did not identify the dominant relaxation mechanism. Instead, they merely state that the field-strength dependence of relaxation anisotropy reflects multiple contributing sources in WM fibers [47]. This inconclusive statement may lead prospective readers to incorrectly infer that a susceptibility-based mechanism governs the observed orientation-dependent R_2 behavior.

Average T_2 (i.e., $1/R_2$) values in WM have also been reported across field strengths ranging from 0.35 T to 9.4 T in two healthy volunteers [49]. When comparing T_2 values at 3 T (62 ± 2 ms) and 7 T (37 ± 3 ms), the susceptibility-related contribution at 3 T is approximately 14%, assuming that the decrease in T_2 with increasing field strength is attributed exclusively to *orientation-dependent* susceptibility-based relaxation pathway. A similar comparison between 3 T and 9.4 T (29 ± 2 ms) yields a susceptibility-related contribution at 3 T of approximately 12%.

To our knowledge, this study represents the first in vivo characterization of orientation-dependent R_2 profiles in human brain WM at 7 T using single SE signals. Previous investigations using formalin-fixed brain samples at 7 T reported minimal orientation dependence in MESE-

St. Jude - Confidential

based R_2 compared to GRE-based R_2^*, leading to the conclusion that susceptibility effects were the primary source of anisotropic transverse relaxation [3]. However, temperature-dependent R_2^* anisotropies observed in the same study pointed to MAE as a more plausible contributor, suggesting that the challenges [50] associated with accurately measuring R_2, particularly at 7 T [51], may obscure the true biophysical origins of orientation-dependent transverse relaxation in WM.

5.3 | B_0-dependent R_2^a from GRE signals

The conclusion regarding the dominant mechanism of anisotropic transverse relaxation in brain WM at 3 T is further supported by GRE-based R_2^a values reported in both the present study and previous investigations across different B_0 field strengths. Notably, this conclusion is strengthened by the consistency of GRE-based R_2^a values observed across studies conducted at varying field strengths. Despite differences in data acquisition and analysis methodologies between two independent studies conducted by separate research groups [40, 41], the GRE-based R_2^a values derived from whole-brain WM at both 3 T (Figure 5A) and 7 T (Figure 5B) in the present study were consistently around 7 s^{-1}. In both investigations, the adverse FAE on orientation-dependent R_2^* profiles were mitigated through linear regression across multiple profiles acquired with different flip angles, as detailed in the literature [41].

When the analysis was focused on specific fiber tracts, such as the corpus callosum (Figure 5C) and the cingulum (Figure 5D) [42], the R_2^a values increased to approximately 10 s^{-1}. However, these elevated values remained statistically indistinguishable between the two B_0 field strengths, suggesting that the observed increases are primarily attributable to relatively higher microstructural anisotropies in these regions. These findings further support the notion that MAE,

St. Jude - Confidential

rather than susceptibility effects, is the dominant contributor to anisotropic transverse relaxation in WM at 3 T.

Comparable GRE-based orientation-dependent R_2 values have been reported across a wide range of B_0 field strengths in a substantial body of literature [13, 24, 25]. In many of these studies, the metric ΔR_2^*, defined as the difference in R_2^* between perpendicular and parallel axonal orientations, is used as a proxy for R_2^a. These values typically range between 3 and 5 s^{-1}. For instance, Rudko et al. [52] reported a ΔR_2^* of approximately 4 s^{-1} in fixed rat brain at 9.4 T, while Wharton et al. [7] found similar values in fresh pig brain at 7 T. In both cases, orientation information was obtained by physically rotating brain samples within the magnet, rather than relying on principal diffusivity directions derived from DTI, thereby providing a more direct assessment of R_2^* orientation dependence.

It is important to note that direct comparisons between the GRE-based R_2^a values reported in the present study and previously published ΔR_2^* values are not strictly meaningful, as the same orientation-dependent R_2^* profile can yield different numerical values depending on the metric used. Nonetheless, the consistent observation of comparable ΔR_2^* values across different species, tissue preparations, and magnetic field strengths provides compelling evidence that MAE is the dominant mechanism underlying anisotropic transverse relaxation at 3 T in brain WM. This conclusion is further supported by recent advances in orientation-dependent relaxation theory [25], which have effectively ruled out susceptibility effects as a plausible primary mechanism for anisotropic transverse relaxation in WM.

6 | CONCLUSIONS

St. Jude - Confidential

This study identifies MAE as the predominant mechanism underlying orientation-dependent transverse relaxation in human brain WM at 3 T, offering a distinct perspective from earlier interpretations in the literature. By disentangling the respective contributions of susceptibility effects and MAE across magnetic field strengths, our findings provide compelling evidence that MAE, rather than susceptibility effects, is the primary drive of the observed anisotropic transverse relaxation behavior at lower fields. These insights carry important implications for advancing the biophysical understanding of anisotropic relaxation contrast in MRI and contribute to a more accurate interpretation of WM microstructure in both clinical and research settings.

DATA AVAILABILITY STATEMENT

Data and Python/IDL scripts used in this work are available upon request from the authors.

CONFLICT OF INTEREST

The author has no conflicts of interest to declare.

FUNDING INFORMATION

This work was partially supported by the American Lebanese Syrian Associated Charities (ALSAC) at St. Jude Children's Research Hospital.

ORCID

Yuxi Pang: https://orcid.org/0000-0001-5039-0236

Wilburn E. Reddick: https://orcid.org/0000-0002-1054-1201

St. Jude - Confidential

REFERENCES

[1] Gore JC, Kennan RP. Physical and physiological basis of magnetic relaxation. Magn Reson Imaging 1999;1:33-42.

[2] Mathur-De Vre R. The NMR studies of water in biological systems. Progress in Biophysics and Molecular Biology 1980;35:103-34.

[3] Oh S-H, Kim Y-B, Cho Z-H, Lee J. Origin of B0 orientation dependent R2*(= 1/T2*) in white matter. Neuroimage 2013;73:71-9.

[4] COPE FW. Unjustified doubts about the nuclear magnetic resonance demonstration of structured water in neural and muscle tissue. Nature New Biology 1972;237(76):215-.

[5] Pang Y. Orientation dependent proton transverse relaxation in human brain white matter: The magic angle effect on a cylindrical helix. Magnetic Resonance Imaging 2023;100:73-83.

[6] Pang Y. Phase shifted transverse relaxation orientation dependences in human brain white matter. NMR Biomed 2023;10.1002/nbm.4925.

[7] Wharton S, Bowtell R. Gradient echo based fiber orientation mapping using R2* and frequency difference measurements. Neuroimage 2013;83:1011-23.

[8] Knight MJ, Dillon S, Jarutyte L, Kauppinen RA. Magnetic resonance relaxation anisotropy: Physical principles and uses in microstructure imaging. Biophys J 2017;112(7):1517-28.

[9] Duyn JH, van Gelderen P, Li T-Q, de Zwart JA, Koretsky AP, Fukunaga M. High-field MRI of brain cortical substructure based on signal phase. Proceedings of the National Academy of Sciences 2007;104(28):11796-801.

[10] Li T-Q, van Gelderen P, Merkle H, Talagala L, Koretsky AP, Duyn J. Extensive heterogeneity in white matter intensity in high-resolution T2*-weighted MRI of the human brain at 7.0 T. Neuroimage 2006;32(3):1032-40.

[11] Wiggins C, Gudmundsdottir V, Le Bihan D, Lebon V, Chaumeil M. Orientation dependence of white matter T2* contrast at 7T: a direct demonstration. In: Proceedings of the International Society of Magnetic Resonance Medicine, Toronto, Canada, 2008. (abstract: 237).

[12] Cherubini A, Péran P, Hagberg GE, Varsi AE, Luccichenti G, Caltagirone C, et al. Characterization of white matter fiber bundles with T2* relaxometry and diffusion tensor imaging. Magn Reson Med 2009;61(5):1066-72.

[13] Bender B, Klose U. The in vivo influence of white matter fiber orientation towards B0 on T2* in the human brain. NMR Biomed 2010;23(9):1071-6.

[14] Denk C, Torres EH, MacKay A, Rauscher A. The influence of white matter fibre orientation on MR signal phase and decay. NMR Biomed 2011;24(3):246-52.

[15] Tax CMW, Kleban E, Chamberland M, Baraković M, Rudrapatna U, Jones DK. Measuring compartmental T(2)-orientational dependence in human brain white matter using a tiltable RF coil and diffusion-T(2) correlation MRI. Neuroimage 2021;236:117967.

[16] Lee J, van Gelderen P, Kuo L-W, Merkle H, Silva AC, Duyn JH. T2*-based fiber orientation mapping. Neuroimage 2011;57(1):225-34.

[17] Bartels LM, Doucette J, Birkl C, Zhang Y, Weber AM, Rauscher A. Orientation dependence of R2 relaxation in the newborn brain. NeuroImage 2022;264:119702.

[18] Lenz C, Berger C, Bauer M, Scheurer E, Birkl C. Sensitivity of fiber orientation dependent R2∗ to temperature and post mortem interval. Magn Reson Med 2021;86(5):2703-15.
[19] Birkl C, Doucette J, Fan M, Hernandez-Torres E, Rauscher A. Myelin water imaging depends on white matter fiber orientation in the human brain. Magn Reson Med 2021;85(4):2221-31.
[20] Wharton S, Bowtell R. Fiber orientation-dependent white matter contrast in gradient echo MRI. Proc Natl Acad Sci USA 2012;109(45):18559-64.
[21] Bydder M, Rahal A, Fullerton GD, Bydder GM. The magic angle effect: a source of artifact, determinant of image contrast, and technique for imaging. J Magn Reson Imaging 2007;25(2):290-300.
[22] Berendsen HJC. Nuclear magnetic resonance study of collagen hydration. J Chem Phys 1962;36(12):3297-305.
[23] Knight MJ, Wood B, Couthard E, Kauppinen R. Anisotropy of spin-echo T2 relaxation by magnetic resonance imaging in the human brain in vivo. Biomed Spectrosc Imaging 2015;4(3):299-310.
[24] Gil R, Khabipova D, Zwiers M, Hilbert T, Kober T, Marques JP. An in vivo study of the orientation‐dependent and independent components of transverse relaxation rates in white matter. NMR Biomed 2016;29(12):1780-90.
[25] Yablonskiy DA, Sukstanskii AL. Quantum magnetization exchange through transient hydrogen bond matrix defines magnetic resonance signal relaxation and anisotropy in central nervous system. Scientific Reports 2025;15(1):23834.
[26] Yablonskiy DA, Haacke EM. Theory of NMR signal behavior in magnetically inhomogeneous tissues: the static dephasing regime. Magn Reson Med 1994;32(6):749-63.
[27] Simons M, Nave K-A. Oligodendrocytes: myelination and axonal support. Cold Spring Harbor perspectives in biology 2016;8(1):a020479.
[28] Beaulieu C. The biological basis of diffusion anisotropy. Diffusion MRI. Elsevier; 2014, p. 155-83.
[29] Cheng J-X, Pautot S, Weitz DA, Xie XS. Ordering of water molecules between phospholipid bilayers visualized by coherent anti-Stokes Raman scattering microscopy. Proc Natl Acad Sci USA 2003;100(17):9826-30.
[30] Grunder W. MRI assessment of cartilage ultrastructure. NMR Biomed 2006;19(7):855-76.
[31] Pang Y. Characterization of anisotropic T2W signals from human knee femoral cartilage: The magic angle effect on a spherical surface. NMR Biomed 2021;34(7):e4535.
[32] Schyboll F, Jaekel U, Weber B, Neeb H. The impact of fibre orientation on T 1-relaxation and apparent tissue water content in white matter. MAGMA 2018;31(4):501-10.
[33] Kauppinen RA, Paasonen E, Thotland J, Könönen M, Pisharady P, Lenglet C, et al. Fiber orientation‐dependent T1 angular features in human white matter at 1.5 T, 3 T, and 7 T. Magnet Reson Med 2025;94(6):2611-23.
[34] Pang Y. An order parameter without magic angle effect (OPTIMA) derived from R1ρ dispersion in ordered tissue. Magn Reson Med 2020;83(5):1783-95.
[35] Mlynarik V, Szomolanyi P, Toffanin R, Vittur F, Trattnig S. Transverse relaxation mechanisms in articular cartilage. J Magn Reson 2004;169(2):300-7.
[36] van Gelderen P, Wang Y, de Zwart JA, Duyn JH. Dependence of brain-tissue R(2) on MRI field strength. Magn Reson Med 2025;93(5):2140-52.

[37] Smith SM, Jenkinson M, Woolrich MW, Beckmann CF, Behrens TE, Johansen-Berg H, et al. Advances in functional and structural MR image analysis and implementation as FSL. Neuroimage 2004;23:S208-S19.
[38] Ennis DB, Kindlmann G. Orthogonal tensor invariants and the analysis of diffusion tensor magnetic resonance images. Magn Reson Med 2006;55(1):136-46.
[39] Markwardt CB. Non-linear least squares fitting in IDL with MPFIT. arXiv preprint arXiv:09022850 2009.
[40] Sibgatulin R, Deistung A, Güllmar D, Birkl C, Ropele S, Reichenbach JR. In vivo assessment of the anisotropy of R2* maps in white matter. In: Proceedings of the International Society of Magnetic Resonance Medicine, Montreal, CA 2019. (abstract: 4906).
[41] Milotta G, Corbin N, Lambert C, Lutti A, Mohammadi S, Callaghan MF. Mitigating the impact of flip angle and orientation dependence in single compartment R2* estimates via 2‐pool modeling. Magn Reson Med 2023;89(1):128-43.
[42] Chen L, Mao D, Gilbert G, Versluis M, van Zijl P, Li X. Orientation dependence of local frequency difference and R2* in parallel versus crossing fibers at 3T and 7T. In: Proceedings of the International Society of Magnetic Resonance Medicine, London, UK, 2022. (abstract: 1643).
[43] Chen L, Shin HG, van Zijl PCM, Li X. Exploiting gradient-echo frequency evolution: Probing white matter microstructure and extracting bulk susceptibility-induced frequency for quantitative susceptibility mapping. Magn Reson Med 2024;91(4):1676-93.
[44] Tournier JD, Calamante F, Connelly A. Robust determination of the fibre orientation distribution in diffusion MRI: non-negativity constrained super-resolved spherical deconvolution. Neuroimage 2007;35(4):1459-72.
[45] Bevington PR, Robinson DK. Data reduction and error analysis for the physical sciences. 3rd ed. Boston: McGraw-Hill; 2003.
[46] Tournier JD, Smith R, Raffelt D, Tabbara R, Dhollander T, Pietsch M, et al. MRtrix3: A fast, flexible and open software framework for medical image processing and visualisation. Neuroimage 2019;202:116137.
[47] Bauer M, Kremser C, Gizewski ER, Lenz C, Birkl C. Field strength dependence reveals multiple sources of relaxation anisotropy in single and crossing white matter fibers. NeuroImage 2025:121394.
[48] Mäkelä HI, De Vita E, Gröhn OH, Kettunen MI, Kavec M, Lythgoe M, et al. B0 dependence of the on‐resonance longitudinal relaxation time in the rotating frame ($T1\rho$) in protein phantoms and rat brain in vivo. Magn Reson Med 2004;51(1):4-8.
[49] Zhu J, Klarhöfer M, Santini F, Scheffler K, Bieri O. Relaxation measurements in brain tissue at field strengths between 0.35 T and 9.4 T. Joint Annual Meeting ISMRM-ESMRMB 2014, (abstract: 3208).
[50] Oliveira Assunção TB, Naji N, Snyder J, Seres P, Blevins G, Smyth P, et al. Importance of R(2) accuracy in susceptibility source separation. Magn Reson Med 2025.
[51] van Gelderen P, Wang Y, de Zwart JA, Duyn JH. Dependence of brain‐tissue R2 on MRI field strength. Magnet Reson Med 2025;93(5):2140-52.
[52] Rudko DA, Klassen LM, de Chickera SN, Gati JS, Dekaban GA, Menon RS. Origins of R2∗ orientation dependence in gray and white matter. Proc Natl Acad Sci USA 2014;111(1):E159-E67.

FIVE FIGURES

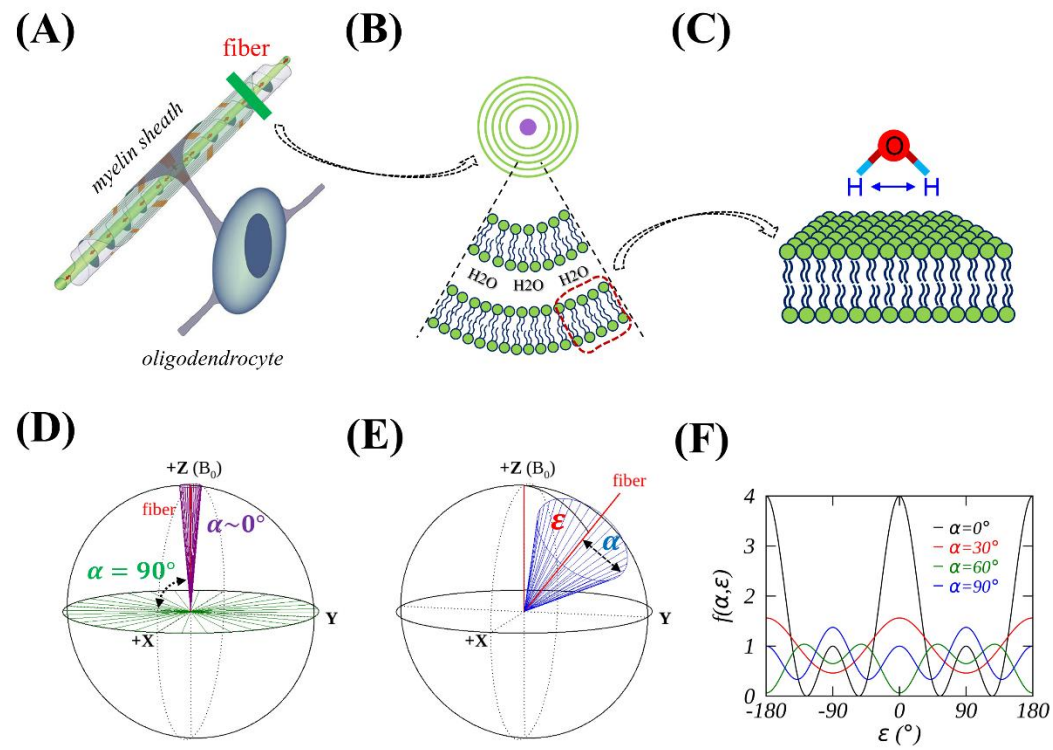

FIGURE 1. *Schematics illustrate the hierarchical structures of rotationally restricted water in an axon fiber and a cone model for orientation-dependent transverse relaxation. (A) Myelinated axon fiber, adapted from Reference 25. (B) Cross-sectional view perpendicular to the fiber, showing restricted water located within the axon (filled violet circle) and in the extra-axonal space (between membrane bilayers). (C) Restricted water molecule near the membrane surface. (D) Restricted water within the axon (α=0°, violet) and outside the axon (α=90°, green). (E) Cone model with an opening angle α, orientated at an angle ε relative to the static magnetic field* B_0*. (F) Theoretical orientation dependence of transverse relaxation. Note: when referring to the orientation of restricted water, this denotes the direction of the residual dipolar interaction between two protons within the water molecule, as schematically illustrated in panel (C).*

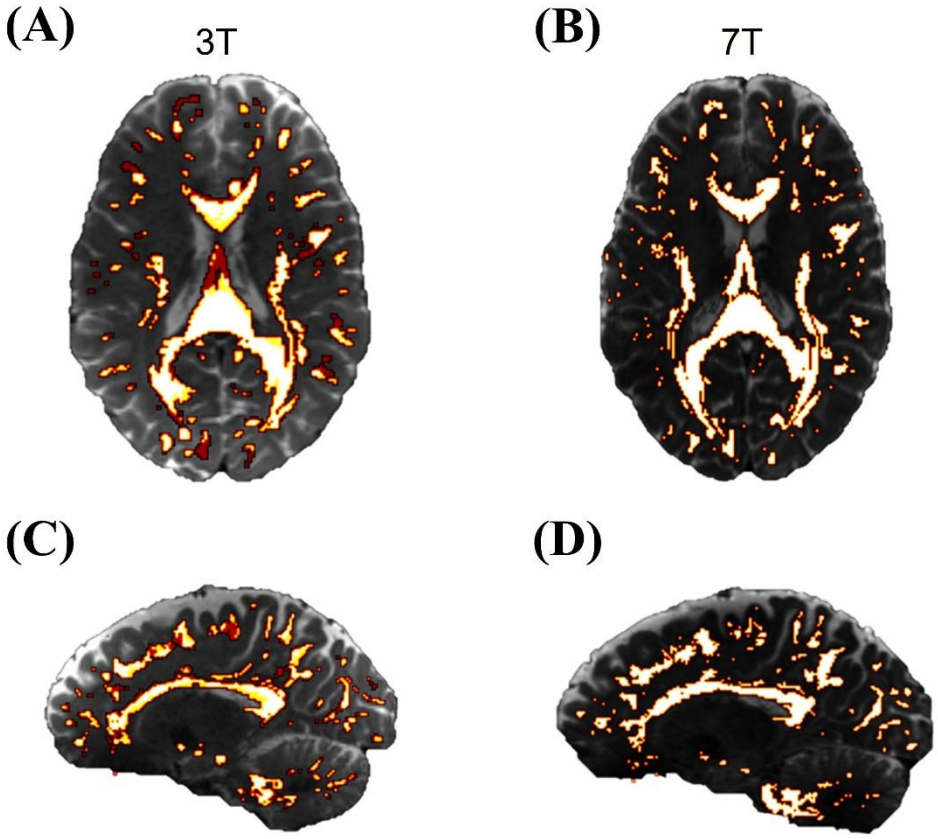

FIGURE 2. *White matter (WM) masks overlaid on T_2-weighted (b-value = 0) images in axial (A, B) and sagittal (C, D) views from 3 T (A, C) and 7 T (B, D) DTI datasets. Although the WM masks are displayed using a continuous colormap for visualization purposes, the underlying data are binary (0 or 1) and were used as such in all analyses.*

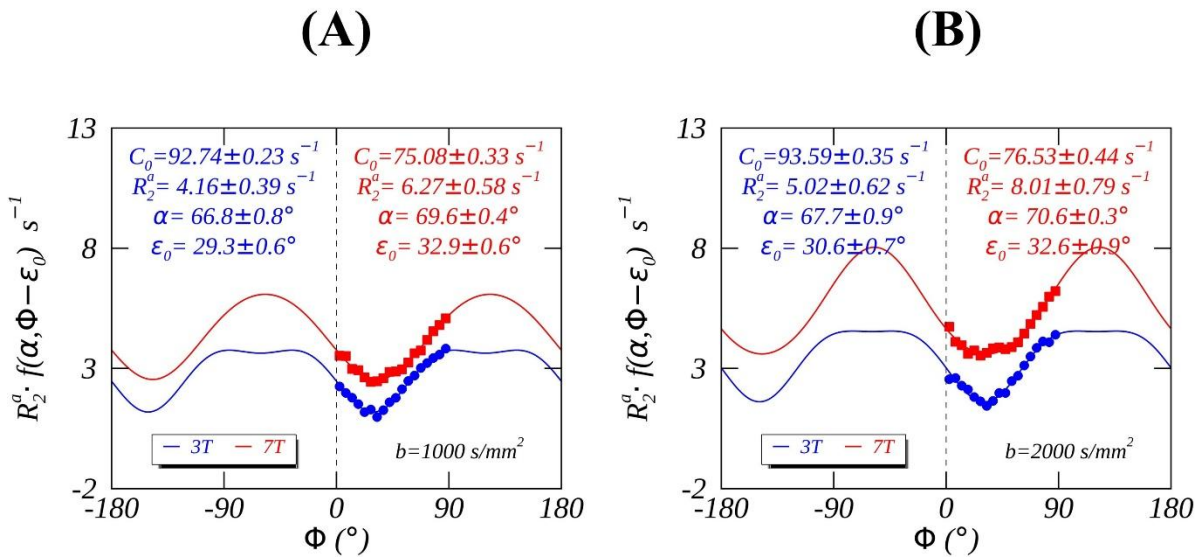

FIGURE 3. *Measured (colored symbols) and fitted (colored lines) orientation-dependent transverse relaxation rates* $R_2^a \cdot f(\alpha, \Phi - \varepsilon_0)$ *from Subject 15 at 3 T (blue) and 7 T (red), based on DTI using non-zero b-values of 1000 s/mm^2 (A) and 2000 s/mm^2 (B).*

St. Jude - Confidential

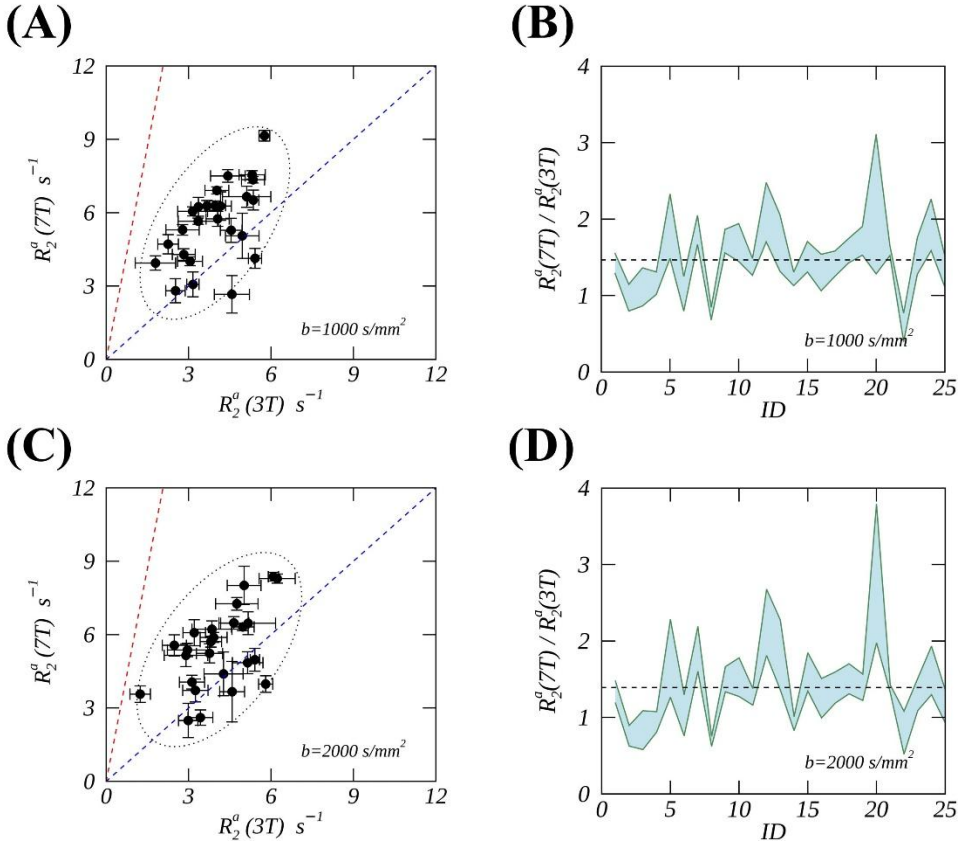

FIGURE 4. *Scatterplots (A, C) and ratio plots (B, D) of derived R_2^a from 7 T and 3 T DTI datasets across 25 subjects. DTI datasets were obtained using non-zero b-values of 1000 s/mm² (A, B) and 2000 s/mm² (C, D). In the scatterplots, colored dashed lines represent the theoretical ratios of $R_2^a(7T)/R_2^a(3T)$ assuming anisotropic transverse relaxation arises from susceptibility effects (red) or the magic angle effect (blue). In the ratio plots, horizontal dashed lines indicate the average ratios measured across the 25 subjects. Note that standard deviations are indicated by error bars (A, C) and by the half-widths of the shaded ribbons (B, D). The ellipses in panels A and C represent the 95% confidence level.*

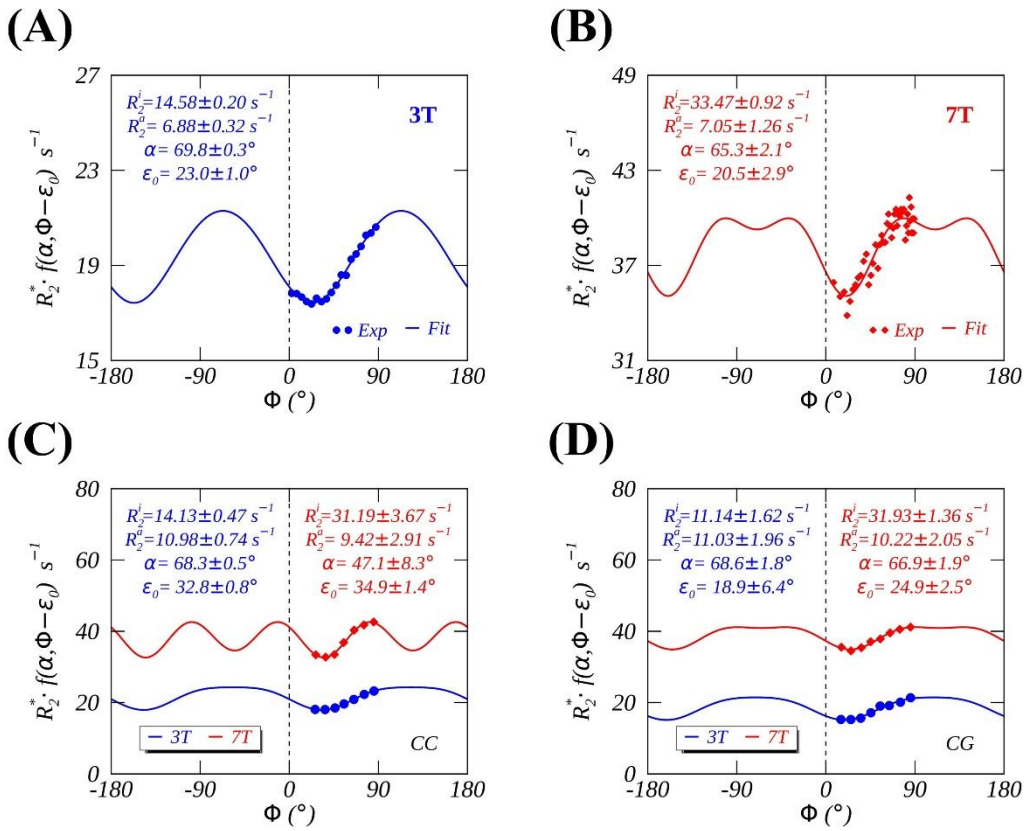

FIGURE 5. *Measured (colored symbols) and fitted (colored lines) orientation-dependent transverse relaxation rates* $R_2^* \cdot f(\alpha, \Phi - \varepsilon_0)$ *at 3 T (blue lines) and 7 T (red lines). Orientation-dependent* R_2^* *profiles were derived from: (A, B) whole brain WM; (C) corpus callosum; and (D) cingulum.*

Supporting Information

TABLE S1. *Fitted parameters from the orientation-dependent transverse relaxation model for 25 subjects, based on DTI datasets acquired with a non-zero b-value of 1000 s/mm² at 3 T and 7 T. Values are presented as mean ± standard deviation.*

Number	HCP_ID	3T (b=1000 s/mm²)				7T (b=1000 s/mm²)			
		C_0 (s^{-1})	R_2^a (s^{-1})	α (°)	ε_0 (°)	C_0 (s^{-1})	R_2^a (s^{-1})	α (°)	ε_0 (°)
1	100610_M28	94.1 ± 0.3	5.3 ± 0.5	68.2 ± 0.7	25.8 ± 0.9	79.7 ± 0.1	7.5 ± 0.2	68.6 ± 0.2	20.0 ± 0.5
2	126426_F33	92.1 ± 0.1	3.2 ± 0.2	68.2 ± 0.5	28.6 ± 0.6	77.0 ± 0.7	3.1 ± 0.5	69.2 ± 2.3	0.9 ± 16.2
3	130114_M28	92.5 ± 0.2	2.5 ± 0.4	60.8 ± 2.7	26.3 ± 0.7	76.5 ± 0.3	2.8 ± 0.5	67.8 ± 1.5	22.7 ± 2.3
4	130518_F33	93.0 ± 0.2	4.5 ± 0.4	66.6 ± 0.8	26.0 ± 0.7	78.6 ± 0.4	5.3 ± 0.5	68.7 ± 0.9	17.1 ± 2.6
5	134627_M28	93.1 ± 0.3	2.8 ± 0.6	63.8 ± 2.6	32.2 ± 0.7	77.5 ± 0.2	5.3 ± 0.2	69.7 ± 0.5	12.3 ± 2.9
6	135124_F33	93.2 ± 0.4	5.0 ± 0.6	68.0 ± 0.9	28.1 ± 1.0	78.5 ± 0.4	5.1 ± 0.9	71.0 ± 2.9	6.4 ± 25.0
7	146735_F33	92.4 ± 0.2	3.4 ± 0.3	68.3 ± 0.6	27.3 ± 0.8	79.2 ± 0.2	6.2 ± 0.4	71.0 ± 0.3	23.5 ± 1.9
8	148133_F28	93.2 ± 0.1	5.4 ± 0.2	68.6 ± 0.3	26.6 ± 0.5	77.5 ± 0.3	4.1 ± 0.4	68.3 ± 0.9	20.8 ± 1.8
9	165436_M28	93.7 ± 0.2	3.7 ± 0.3	66.2 ± 0.8	23.7 ± 0.7	79.9 ± 0.2	6.3 ± 0.2	70.5 ± 0.3	0.0 ± 0.0
10	167440_F28	92.1 ± 0.4	4.4 ± 0.6	68.0 ± 1.1	25.1 ± 1.5	81.6 ± 0.2	7.5 ± 0.3	70.3 ± 0.3	0.0 ± 0.0
11	177140_F33	95.5 ± 0.3	5.3 ± 0.4	67.9 ± 0.6	23.8 ± 0.9	82.6 ± 0.1	7.3 ± 0.1	71.9 ± 0.1	0.0 ± 0.0
12	180533_F33	92.2 ± 0.2	2.3 ± 0.4	61.1 ± 2.9	30.3 ± 0.6	78.1 ± 0.2	4.7 ± 0.4	67.5 ± 0.7	22.6 ± 1.0
13	193845_M28	92.4 ± 0.4	3.3 ± 0.7	63.9 ± 2.5	33.5 ± 0.7	78.2 ± 0.1	5.7 ± 0.1	70.6 ± 0.4	9.2 ± 3.3
14	360030_F33	94.4 ± 0.2	5.4 ± 0.2	69.1 ± 0.4	14.4 ± 1.6	78.2 ± 0.3	6.5 ± 0.4	69.3 ± 0.5	0.0 ± 0.0
15	385046_M28	92.7 ± 0.2	4.2 ± 0.4	66.8 ± 0.8	29.3 ± 0.6	75.1 ± 0.3	6.3 ± 0.6	69.6 ± 0.4	32.9 ± 0.6
16	401422_F33	94.4 ± 0.5	5.1 ± 0.9	69.0 ± 1.1	27.6 ± 1.8	80.8 ± 0.3	6.7 ± 0.4	70.2 ± 0.4	26.0 ± 1.2
17	463040_F33	92.8 ± 0.3	4.1 ± 0.4	67.7 ± 0.8	25.4 ± 1.0	79.0 ± 0.3	5.7 ± 0.3	70.8 ± 1.3	3.2 ± 10.5
18	644246_F33	93.5 ± 0.2	4.0 ± 0.4	67.8 ± 0.8	23.9 ± 1.1	80.0 ± 0.2	6.3 ± 0.2	68.7 ± 0.3	12.8 ± 1.3
19	654552_F33	93.8 ± 0.3	4.0 ± 0.4	66.9 ± 1.0	24.6 ± 1.0	79.9 ± 0.1	6.9 ± 0.1	69.9 ± 0.3	11.0 ± 2.0
20	757764_F36	91.0 ± 0.4	1.8 ± 0.7	62.3 ± 6.4	27.1 ± 2.0	77.3 ± 0.2	3.9 ± 0.3	71.9 ± 0.6	0.0 ± 0.0
21	765864_F28	95.6 ± 0.1	5.8 ± 0.2	68.0 ± 0.3	19.2 ± 0.7	82.7 ± 0.2	9.1 ± 0.2	71.5 ± 0.2	0.0 ± 0.0
22	878877_M28	92.6 ± 0.4	4.6 ± 0.6	66.7 ± 1.2	27.4 ± 1.0	71.7 ± 0.4	2.7 ± 0.8	63.5 ± 3.5	34.2 ± 0.8
23	905147_F36	92.2 ± 0.3	2.8 ± 0.4	66.9 ± 1.4	23.3 ± 1.5	77.1 ± 0.2	4.3 ± 0.2	69.3 ± 0.4	0.0 ± 0.0
24	943862_M28	93.4 ± 0.3	3.1 ± 0.5	65.9 ± 1.7	28.7 ± 0.9	79.4 ± 0.2	6.1 ± 0.2	68.1 ± 0.3	11.9 ± 1.1
25	971160_M28	93.6 ± 0.3	3.1 ± 0.5	64.9 ± 1.7	26.4 ± 0.9	78.2 ± 0.1	4.0 ± 0.2	71.8 ± 0.4	0.0 ± 0.0
mean ± std		93.2 ± 1.1	4.0 ± 1.1	66.5 ± 2.3	26.2 ± 3.8	78.6 ± 2.3	5.6 ± 1.6	69.6 ± 1.8	11.5 ± 11.0

St. Jude - Confidential

TABLE S2. *Fitted parameters from the orientation-dependent transverse relaxation model for 25 subjects, based on DTI datasets acquired with a non-zero b-value of 2000 s/mm² at 3 T and 7 T. Values are reported as mean ± standard deviation.*

Number	HCP_ID	3T (b=2000 s/mm²)				7T (b=2000 s/mm²)			
		C_0 (s^{-1})	R_2^a (s^{-1})	α (°)	ε_0 (°)	C_0 (s^{-1})	R_2^a (s^{-1})	α (°)	ε_0 (°)
1	100610_M28	94.8 ± 0.4	6.2 ± 0.7	69.1 ± 0.7	27.1 ± 1.2	80.6 ± 0.1	8.3 ± 0.2	69.6 ± 0.2	21.5 ± 0.6
2	126426_F33	92.3 ± 0.3	3.4 ± 0.4	68.9 ± 0.8	29.8 ± 1.1	76.9 ± 0.2	2.6 ± 0.3	69.1 ± 1.0	0.0 ± 0.0
3	130114_M28	92.8 ± 0.2	3.0 ± 0.4	62.1 ± 1.8	28.5 ± 0.5	76.8 ± 0.4	2.5 ± 0.7	66.5 ± 2.2	33.8 ± 1.0
4	130518_F33	93.4 ± 0.3	5.1 ± 0.6	67.6 ± 0.9	26.9 ± 0.9	78.4 ± 0.3	4.8 ± 0.4	68.9 ± 0.8	18.7 ± 2.4
5	134627_M28	93.3 ± 0.4	2.9 ± 0.8	63.5 ± 3.3	34.2 ± 0.8	78.0 ± 0.1	5.2 ± 0.5	71.4 ± 1.0	7.1 ± 8.5
6	135124_F33	92.9 ± 0.4	4.3 ± 0.7	67.1 ± 1.3	29.3 ± 1.0	78.2 ± 0.5	4.4 ± 0.9	70.9 ± 3.6	5.4 ± 30.9
7	146735_F33	92.4 ± 0.2	3.2 ± 0.4	67.8 ± 0.9	30.3 ± 0.8	79.4 ± 0.2	6.1 ± 0.5	71.7 ± 0.4	19.4 ± 4.0
8	148133_F28	93.5 ± 0.2	5.8 ± 0.3	69.2 ± 0.3	26.6 ± 0.5	77.6 ± 0.2	4.0 ± 0.3	69.5 ± 0.7	19.8 ± 2.4
9	165436_M28	93.9 ± 0.2	3.8 ± 0.4	66.6 ± 1.0	25.1 ± 0.9	79.7 ± 0.2	5.7 ± 0.2	70.7 ± 0.3	0.0 ± 0.0
10	167440_F28	92.4 ± 0.5	4.8 ± 0.8	68.5 ± 1.2	26.1 ± 1.8	81.5 ± 0.2	7.3 ± 0.3	70.5 ± 0.3	0.0 ± 0.0
11	177140_F33	95.4 ± 0.3	5.0 ± 0.4	67.6 ± 0.7	25.1 ± 0.8	82.1 ± 0.1	6.3 ± 0.2	71.7 ± 0.2	0.0 ± 0.0
12	180533_F33	92.5 ± 0.2	2.5 ± 0.4	62.5 ± 2.5	31.5 ± 0.6	78.9 ± 0.3	5.6 ± 0.4	69.1 ± 0.6	22.3 ± 1.5
13	193845_M28	92.4 ± 0.4	3.0 ± 0.7	61.7 ± 3.7	35.0 ± 0.6	78.4 ± 0.1	5.4 ± 0.3	71.9 ± 0.4	5.9 ± 3.5
14	360030_F33	94.6 ± 0.1	5.4 ± 0.2	69.5 ± 0.3	14.5 ± 1.6	77.8 ± 0.3	5.0 ± 0.5	69.3 ± 0.8	0.0 ± 0.0
15	385046_M28	93.6 ± 0.4	5.0 ± 0.6	67.7 ± 0.9	30.6 ± 0.7	76.5 ± 0.4	8.0 ± 0.8	70.6 ± 0.3	32.6 ± 0.9
16	401422_F33	94.6 ± 0.6	5.2 ± 1.0	69.2 ± 1.1	28.5 ± 1.9	81.1 ± 0.3	6.5 ± 0.5	71.1 ± 0.3	25.1 ± 1.9
17	463040_F33	92.8 ± 0.3	3.8 ± 0.5	66.9 ± 1.1	27.5 ± 0.9	78.8 ± 0.3	5.2 ± 0.4	70.9 ± 1.6	2.0 ± 13.2
18	644246_F33	93.6 ± 0.3	3.9 ± 0.5	67.9 ± 1.0	25.3 ± 1.3	80.0 ± 0.2	5.9 ± 0.2	69.4 ± 0.5	9.8 ± 2.6
19	654552_F33	94.3 ± 0.3	4.6 ± 0.5	67.7 ± 0.9	27.2 ± 1.0	80.3 ± 0.1	6.5 ± 0.3	71.5 ± 0.5	2.7 ± 3.9
20	757764_F36	91.0 ± 0.5	1.2 ± 0.4	49.6 ± 14.0	29.6 ± 2.1	77.3 ± 0.2	3.6 ± 0.3	71.8 ± 0.8	0.0 ± 0.0
21	765864_F28	95.9 ± 0.1	6.1 ± 0.2	68.3 ± 0.3	20.3 ± 0.6	82.4 ± 0.1	8.4 ± 0.2	72.0 ± 0.2	0.0 ± 0.0
22	878877_M28	93.0 ± 0.3	4.6 ± 0.5	66.2 ± 0.9	30.4 ± 0.5	72.7 ± 0.7	3.7 ± 1.2	67.0 ± 2.4	35.2 ± 1.2
23	905147_F36	92.5 ± 0.3	3.1 ± 0.5	68.0 ± 1.2	24.8 ± 1.6	77.2 ± 0.2	4.1 ± 0.3	68.9 ± 0.6	0.0 ± 0.0
24	943862_M28	93.9 ± 0.4	3.9 ± 0.7	65.9 ± 1.7	32.6 ± 0.7	80.0 ± 0.3	6.2 ± 0.3	69.5 ± 0.7	13.0 ± 3.3
25	971160_M28	93.8 ± 0.3	3.2 ± 0.5	65.3 ± 1.5	27.8 ± 0.8	78.1 ± 0.2	3.7 ± 0.5	72.1 ± 1.0	5.4 ± 7.6
mean ± std		93.4 ± 1.1	4.1 ± 1.2	66.2 ± 4.0	27.8 ± 4.1	78.7 ± 2.1	5.4 ± 1.6	70.2 ± 1.5	11.2 ± 11.7

St. Jude - Confidential